International Journal of Applied Earth Observations and Geoinformation 116 (2023) 103175

Contents lists available at ScienceDirect

International Journal of Applied Earth Observations and Geoinformation

journal homepage: www.elsevier.com/locate/jag

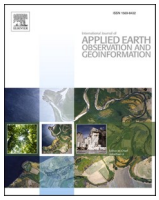

Assessing GEDI-NASA system for forest fuels classification using machine learning techniques

Raúl Hoffrén [a,*], María Teresa Lamelas [a,b], Juan de la Riva [a], Darío Domingo [a,c], Antonio Luis Montealegre [a,b], Alberto García-Martín [a,b], Sergio Revilla [d]

[a] Geoforest-IUCA, Department of Geography and Land Management, University of Zaragoza, Pedro Cerbuna 12, 50009 Zaragoza, Spain
[b] Centro Universitario de la Defensa, Academia General Militar, Ctra. de Huesca s/n, 50090 Zaragoza, Spain
[c] EiFAB-iuFOR, University of Valladolid, Campus Duques de Soria, 42004 Soria, Spain
[d] Instituto Geográfico de Aragón, María Agustín 36, Ed. Pignatelli, 50071 Zaragoza, Spain

ARTICLE INFO

Keywords:
Full-waveform LiDAR
Landsat-8 OLI
Mediterranean ecosystems
Prometheus
SVM
Random Forest

ABSTRACT

Identification of forest fuels is a key step for forest fire prevention since they provide valuable information of fire behavior. This study assesses NASA's Global Ecosystem Dynamics Investigation (GEDI) system to classify fuel types in Mediterranean environments according to the *Prometheus* model in a forested area of NE Spain. We used 59,554 GEDI footprints and extracted variables related to height metrics, canopy profile metrics, and aboveground biomass density estimates from products L2A, L2B, and L4A, respectively. Four quality filters were applied to discard high uncertainty data, reducing the initial footprints to 9,703. Spectral indices from Landsat-8 OLI scenes were created to test the effect of their integration with GEDI variables on fuel types estimation. Ground-truth data were comprised of *Prometheus* fuel types estimated in two previous studies. Only the types that matched in each GEDI footprint in both studies were used, resulting in a final sample of 1,112 footprints. Spearman's correlation coefficient, Kruskal-Wallis and Dunn's tests determined the variables to be included in the classification models: the relative height at the 85th percentile, the Plant Area Index, and the Aboveground Biomass Density from GEDI, and the brightness from Landsat-8 OLI. Best performances were achieved with Random Forest (RF) and Support Vector Machine with radial kernel (SVM-R), which were lower including only GEDI variables (accuracies: RF and SVM-R = 61.54 %) than integrating the brightness from Landsat-8 OLI (accuracies: RF = 83.71 %, SVM-R = 81.90 %). These results allow validating GEDI for fuel type classification of *Prometheus* model, constituting a promising information for forest management over large areas.

1. Introduction

One of the most common worldwide disturbances of forests are wildfires. In particular, Mediterranean ecosystems are recurrently affected by forest fires, averaging 45,000 events yearly (Oliveira et al., 2012), which produce negative environmental effects, such as soil erosion, biodiversity loss, or greenhouse effect increase. Thus, it is essential to understand fire behavior to help forest managers prevent forest fires and evaluate fire risk over population. In this sense, forest fuels provide valuable information on fire spread and intensity, as they determine the fire regime (Flannigan et al., 2000). In addition, forest fuels represent all the organic matter available for combustion in a forest fire and are the only driver that can be quantified to assess fire risk (Ferraz et al., 2016). In general, forest fuels are classified into different fuel types based mainly on the height and density of vegetation, presenting similar fire behavior (Huesca et al., 2019). Several fuel type classifications have been developed in last decades, most of them in USA and Canada, such as the *Rothermel* fire-spread model (Rothermel, 1972) or the Northern Forest Fire Laboratory (NFFL) model (Albini, 1976). The *Prometheus* model (Prometheus, 1999) adapts the NFFL fuel types to Mediterranean environments (Riaño et al., 2002), considering vegetation height and density as the main fire spreaders and comprising seven categories: one for grassland (FT1), three for shrublands (FT2, FT3, FT4), and three for woodlands (FT5, FT6, FT7) (Table 1).

Remote sensing, specifically LiDAR (*Light Detection and Ranging*) technology, is particularly useful for classifying forest fuels, as they are capable of modelling forest features such as vegetation height, crown density, or biomass volume (Revilla et al., 2021). Furthermore,

* Corresponding author.
E-mail address: rhoffren@unizar.es (R. Hoffrén).

https://doi.org/10.1016/j.jag.2022.103175
Received 29 July 2022; Received in revised form 21 December 2022; Accepted 28 December 2022
1569-8432/© 2022 Published by Elsevier B.V. This is an open access article under the CC BY-NC-ND license (http://creativecommons.org/licenses/by-nc-nd/4.0/).

Table 1
Prometheus fuel types classification.

Fuel Type	Main fire carrier	Cover	Shrub mean height	Vertical difference between shrubs and trees
FT1	Grass	> 60 % grass		
FT2	Shrubs	> 60 % grass and < 50 % trees (>4m)	0.30 – 0.60 *m*	
FT3			0.60 – 2.00 *m*	
FT4			2.00 – 4.00 *m*	
FT5	Trees	< 30 % shrub and > 50 % trees (>4 m)		
FT6		> 30 % shrub and > 50 % trees (>4 m)		> 0.5 *m*
FT7				< 0.5 *m*

integration of LiDAR data with multispectral imagery can provide an improvement in forest fuel model classification (e.g., Domingo et al., 2020; García et al., 2011; Marino et al., 2016). Several studies have used spaceborne LiDAR sensors for forest fuel estimation. For instance, the NASA's Geoscience Laser Altimeter System (GLAS) was used to estimate fire fuel models (e.g., Ashworth et al., 2010), canopy fuel properties for crown fire behavior (e.g., García et al., 2012), and canopy structure and fuel data (e.g., Peterson et al., 2013). The NASA's Advanced Topographic Laser Altimeter System (ATLAS) instrument, launched in 2018, can also be used for vegetation characterization (Narine et al., 2020), although few studies have been conducted to date (e.g., Jiang et al., 2021; Lin et al., 2020; Narine et al., 2019) and none of them on the estimation of forest fuels. However, it should be noted that both GLAS and ATLAS systems were not initially optimized for vegetation and forest structure characterization (Leite et al., 2022, Potapov et al., 2021). The NASA's Global Ecosystem Dynamics Investigation (GEDI), launched in late 2018, is the first spaceborne full-waveform LiDAR system capable of measuring forest vertical structure (Lang et al., 2021; Silva et al., 2021). GEDI differentiates from others spaceborne LiDAR systems in its penetration capability in dense vegetation (Leite et al., 2022), reported in up to ~ 99 % canopy cover (Duncanson et al., 2020; Hancock et al., 2019). GEDI system has been used in recent studies to estimate forest attributes (e.g., Fayad et al., 2021b; Potapov et al., 2021; Rishmawi et al., 2021), biomass (e.g., Duncanson et al., 2020; Puletti et al., 2020; Silva et al., 2021), vegetation height growth dynamics (Guerra-Hernández & Pascual, 2021), and its accuracy for canopy height and above-ground biomass estimates have been assessed (e.g., Dorado-Roda et al., 2021; Fayad et al., 2021a; Lang et al., 2021). However, until now, research concerning forest fuels using GEDI have only been conducted by Leite et al. (2022), who specifically focused on fuel loads in a Brazilian savanna region. Thus, the capability of GEDI for the estimation of fuel types has not yet been evaluated, even though it could help to improve their identification and classification. Data collected by GEDI provide valuable large-scale information that can be used freely and efficiently by users, instead of costly regional and/or national initiatives. It could also support other remote sensing data sources which have proven to be efficient for forest fuels modelling, such as multispectral imagery, Airborne Laser Scanner (ALS) systems, unmanned aerial vehicles, or other current and future satellite LIDAR systems.

In this context, the overall goal of our study is to assess the capability of GEDI to estimate *Prometheus* fuel types in a Mediterranean forest environment by means of Machine Learning classification techniques. Our main hypothesis is that GEDI is able to estimate *Prometheus* fuel types, constituting a valuable information for forest fire prevention at large spatial scales in Mediterranean ecosystems, especially in areas where there is a lack of other LiDAR data to work with. To this end, in order to overcome the high uncertainty in location and poor signal quality of some footprints of GEDI data (Dubayah et al., 2020a), we especially focus on the filtering process of the data to obtain a highest accurate sample to work with. In addition, we test the effect of integrating spectral indices from Landsat-8 Operational Land Imager (OLI) multispectral imagery into the GEDI data to improve the classification of forest fuels.

2. Materials and methods

To reach the objectives we have developed a methodology for the selection of the highest quality GEDI footprints and their integration with multispectral imagery from Landsat-8 OLI. Then, we have assigned the ground-truth to each footprint, consisting in *Prometheus* fuel types mapped in two previous studies. After that, we have selected the most relevant GEDI variables, which have been finally introduced in the classification models using Machine Learning techniques. Fig. 1 synthetizes in a scheme the methodological steps developed in this study.

2.1. Study area

The study was carried out in the central sector of the Ebro Valley, located in the Autonomous Community of Aragon in Northeast Spain (41°51′ N, 0°56′ W) (Fig. 2). The climate of the area is semi-arid, with low and irregular annual precipitations, averaging 350 mm yearly. The annual temperature is ~ 14 °C, with high daily and interseasonal temperature gradient. The study area is mostly placed inside the Military Training Center 'San Gregorio', owned by the Ministry of Defense of Spain. The main land covers include grassland, shrublands, and natural forest of Aleppo pine (*Pinus halepensis* Mill.) with understory dominated by kermes oaks (*Quercus coccifera*), cade junipers (*Juniperus oxycedrus*), thymes (*Thymus vulgaris*), and rosemary (*Rosmarinus officinalis*) (Montealegre et al., 2016).

2.2. GEDI data processing

GEDI began collecting data worldwide in April 2019 between the 51.6° N and 51.6°S latitudes (Dubayah et al., 2020b). The instrument, onboard the International Space Station, is equipped with 3 lasers operating in the near infrared region (1,064 nm). One of the lasers is split into two coverage beams while the other two are full-power beams. The 4 beams are dithered across track to produce a total of 8 beam ground transects of footprints of 25 m diameter, separated 60 m and 600 m along-track and cross-track, respectively. To perform this study, we have used information stored in footprint data sets with three processing levels:: Level 2A Elevation and Height Metrics Data, Version 2 (L2A) (Dubayah et al., 2021a), Level 2B Canopy Cover and Vertical Profile Metrics Data, Version 2 (L2B) (Dubayah et al., 2021b), and Level 4A Aboveground Biomass Density, Version 2.1 (L4A) (Dubayah et al., 2022), which also provide a set of quality flags that allow filtering footprints with high geolocation uncertainty, poor signal quality, and shots affected by atmospheric noise and cloud cover (Dubayah et al., 2020a). The L2A product includes relative height metrics in 100 height intervals or percentiles (RH0, RH1… RH100). The L2B product contains canopy profile metrics: the total Plant Area Index (PAI), the vertical Plant Area Volume Density profile (PAVD), the Foliage Height Diversity index (FHD), and the Total Canopy Cover (TCC). The L4A product stores estimations of above-ground biomass density (AGBD) derived from the L2A data. The L2A and L2B products have been processed from the Level 1B Geolocated Waveform Data, Version 2 (L1B) (Dubayah et al., 2021c) corrected waveforms using six different algorithm setting groups as a result of different processing of the L1B waveforms and noise thresholds. Therefore, for each product there are six different data versions. Nevertheless, this study focuses on the first algorithm setting group, which works properly in the majority of cases (Dubayah et al., 2020a) as it uses conservative thresholds for the waveform signal (Roy et al., 2021). A total of 59,554 footprints stored in 45 orbit tracks registered between April 2019 and December 2021 in our study area were used. To

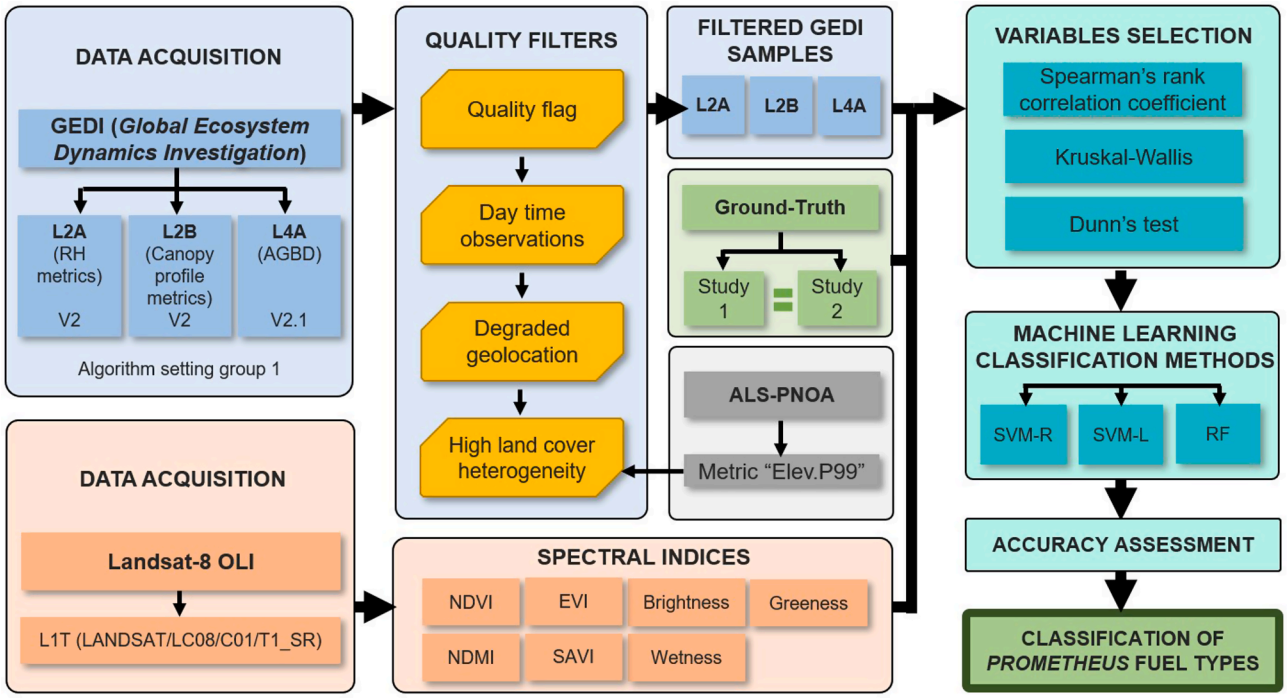

Fig. 1. Synthetic scheme of the methodology followed in this study.

download and process all GEDI data the 4.0.3 version of R environment (R Core Team, 2020) and the 'rGEDI' package (Silva et al., 2020) were used, while the L4A data were downloaded using NASA-Earth Data platform (https://search.earthdata.nasa.gov, accessed 28 Mar 2022). GEDI footprints within our study area were delineated by obtaining their centroid from the geolocated XY data of the L2A product. Since RH variables consists of 100 height percentiles, we arbitrary reduced its initial number by selecting only RH variables every 5 percentiles from RH0 to RH95 along with RH98, RH99, and RH100, in order to reduce time costs in processing in the following stages of the study.

Waveforms from a spaceborne LiDAR system are recurrently affected by cosmic/solar noise, the Earth's atmosphere, and cloud cover, which disturb the quality of the laser signal all the way from the sensor to the ground, affecting derived estimations such as height metrics and biomass estimations. In order to gather a sample with the highest quality, four filters were applied to GEDI data. First, footprints with the 'quality flag' attribute classified as 0 were discarded, meaning that laser shot does not meet the minimum quality requirements based on energy and amplitude (Dubayah et al., 2021c), and that the beam sensitivity has insufficient power to penetrate to the ground (Hofton et al., 2019). Second, observations acquired at day time were rejected to avoid negative impact of solar noise on GEDI waveforms (Potapov et al., 2021). Third, following Roy et al. (2021), samples with potential degraded geolocation were rejected based on the 'degrade flag' attribute. Finally, due to the geolocation uncertainty of GEDI data, in order to ensure the homogeneity in fuel type of GEDI footprints, shots with high land cover heterogeneity were disregarded using ALS information. For this, we used the 99th percentile of the canopy height as reference metric ("Elev. P99"), as one of the main bases of Prometheus fuel types is the height of vegetation. "Elev.P99" was derived from public ALS data from the Spanish National Plan for Aerial Orthophotography (PNOA), captured between 15 October and 16 November 2016. To create "Elev. P99" we removed noise and overlapping returns. Then, following Montealegre et al. (2015a, 2015b), ground points were classified using the MCC 2.1 command-line tool (Evans & Hudak, 2007) and interpolated using a TIN interpolation method (Renslow, 2013) to generate a Digital Elevation Model (DEM) of 1 m spatial resolution. We normalized return heights by subtracting DEM heights using FUSION/LDV 4.21 open-source software (McGaughey, 2009) and extracted the "Elev. P99" metric, which was then rasterized at 10 m spatial resolution. We established this pixel size in order to gather a sufficient number of returns from the low-density ALS-PNOA point-cloud (Gelabert et al., 2020). Then, the spatialized "Elev.P99" metric was extracted to each GEDI footprint by applying a buffer to avoid geolocation error in GEDI data. We used a circular buffer of 30 m radius, as for release versions 2 and 2.1 it is reported a geolocation error of about 10.2 m (Dubayah et al., 2021c). In this way, we ensure that we cover all the spatial uncertainty in the footprints, since the geolocation error can occur in any direction, thus extending the uncertainty to>20 m, considering the 10 m spatial resolution of the spatialized "Elev.P99" metric. Finally, we filtered out footprints with high heterogeneity at the 99th percentile (i.e., significant differences in "Elev.P99" pixel values), which indicates that the footprint does not have homogeneous land cover. For this purpose, we defined as a threshold the standard deviation greater than the 8th decile. Therefore, footprints with a standard deviation of "Elev. P99" pixel values higher than the defined threshold were labeled as heterogeneous in land cover and thus discarded. These filtering processes reduced the number of footprints to 9,703, a 16 % of the initial sample (Table 2), as observed in Fig. 3.

2.3. Landsat-8 OLI data and spectral indices

Landsat-8 OLI images were used to produce seven spectral indices. The OLI instrument began collecting data in April 2013 in the visible and infrared spectral regions, and includes a panchromatic band. In this study, we used the visible and near infrared bands of 30 m spatial resolution from the terrain-corrected scenes (L1T: "LANDSAT/LC08/C01/T1_SR"). Monthly images from June, July, and August 2019, 2020, and 2021 with less cloud cover than 10 % were selected for the study area and processed through Google Earth Engine (GEE) (Gorelick et al., 2017). The seven spectral indices produced were: the Normalized Difference Vegetation Index (NDVI) (Eq. (1), Rouse et al., 1974), the Normalized Difference Moisture Index (NDMI) (Eq. (2), Masek et al., 2006), the Enhanced Vegetation Index (EVI) (Eq., Liu & Huete, 1995), the Soil Adjusted Vegetation Index (SAVI) (Eq. (4), Huete, 1988), brightness, greenness, and wetness of the Tasseled Cap transformation

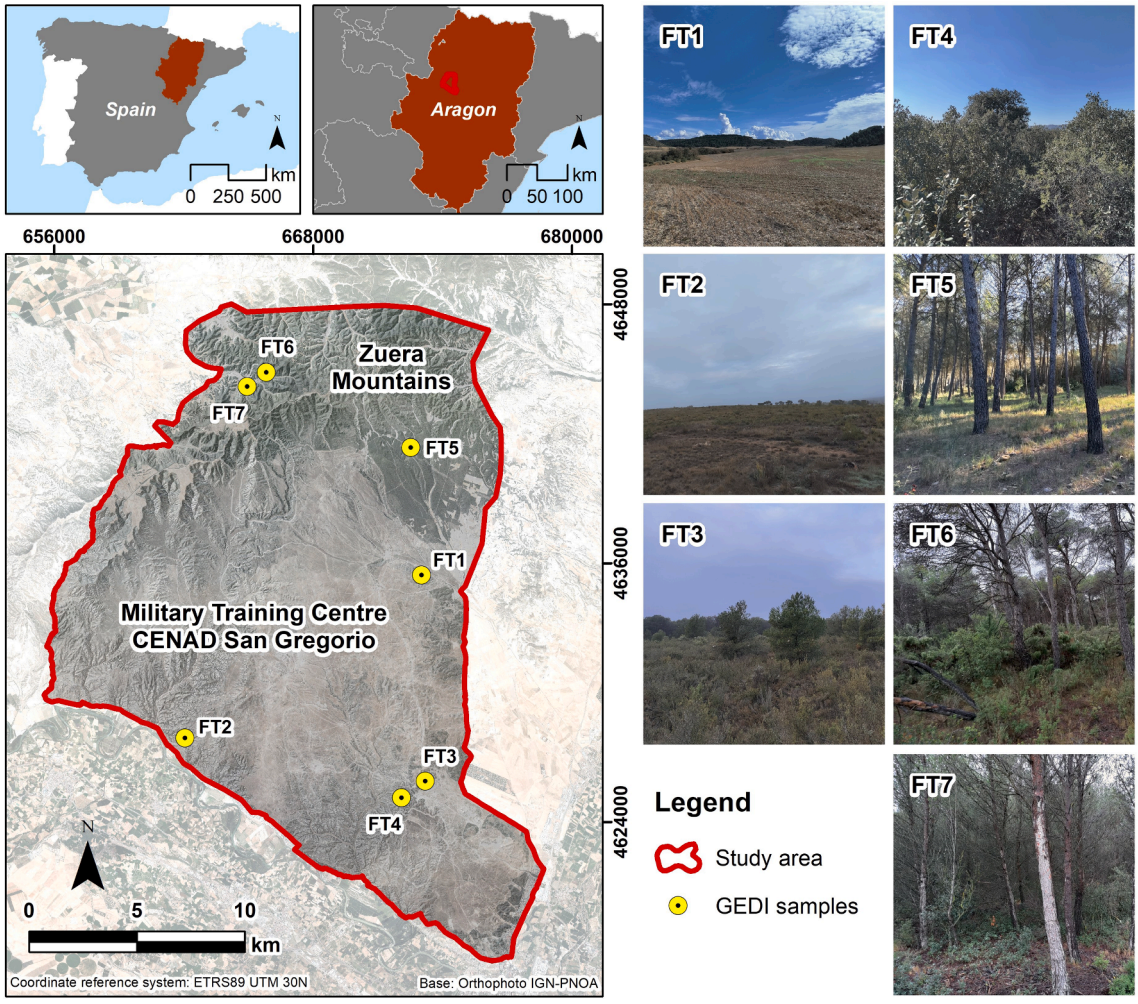

Fig. 2. Study area on the central sector of the Ebro Valley, in Aragon (NE Spain), and examples of each *Prometheus* fuel type within a selection of GEDI footprints.

Table 2
Sequentially reduction of the number of GEDI footprints and percentage of remaining footprints by filter applied.

	Initial footprints	Filter 1: Quality Flag	Filter 2: Day time observations	Filter 3: Degraded geolocation	Filter 4: High land cover heterogeneity	Footprints Remaining
Number of footprints	**59,554**	−37,532	−9,240	−96	−2,983	**9,703**
Percentage of remaining footprints	**100 %**	37 %	22 %	21 %	16 %	**16 %**

(Eqs. (5)–(7), Kauth & Thomas, 1976). The GEE code developed for this study was a modification of the original by Decuyper et al. (2022).

$$NDVI = \frac{NIR - R}{NIR + R} \quad (1)$$

$$NDMI = \frac{NIR - SWIR1}{NIR + SWIR1} \quad (2)$$

$$EVI = 2.5 \times \frac{NIR - R}{(NIR + 6 \times R - 7.5 \times B) + 1} \quad (3)$$

$$SAVI = \frac{NIR - R}{(NIR + R + 0.5)} \times (1 + 0.5) \quad (4)$$

$$Brightness = 0.3029 \times B + 0.2786 \times G + 0.4733 \times R + 0.5599 \times NIR + 0.508 \times SWIR1 + 0.1872 \times SWIR2 \quad (5)$$

$$Greenness = -0.2941 \times B - 0.243 \times G - 0.5424 \times R + 0.7276 \times NIR + 0.0713 \times SWIR1 - 0.1608 \times SWIR2 \quad (6)$$

$$Wetness = 0.1511 \times B + 0.1973 \times G + 0.3283 \times R + 0.3407 \times NIR - 0.7117 \times SWIR1 - 0.4559 \times SWIR2 \quad (7)$$

Where NDVI is the Normalized Difference Vegetation Index, NDMI is the Normalized Difference Moisture Index, EVI is the Enhanced Vegetation Index, SAVI is the Soil Adjusted Vegetation Index, SWIR1 is the shortwave infrared band 6, NIR is the near infrared band, R is the red band, G is the green band, and B is the blue band.

From the initial 9 images of each spectral index, we calculated their maximum value to create a single composite image that better capture the vegetative period variability. Finally, from each composite image we calculated the mean value of all pixels within each GEDI footprints for

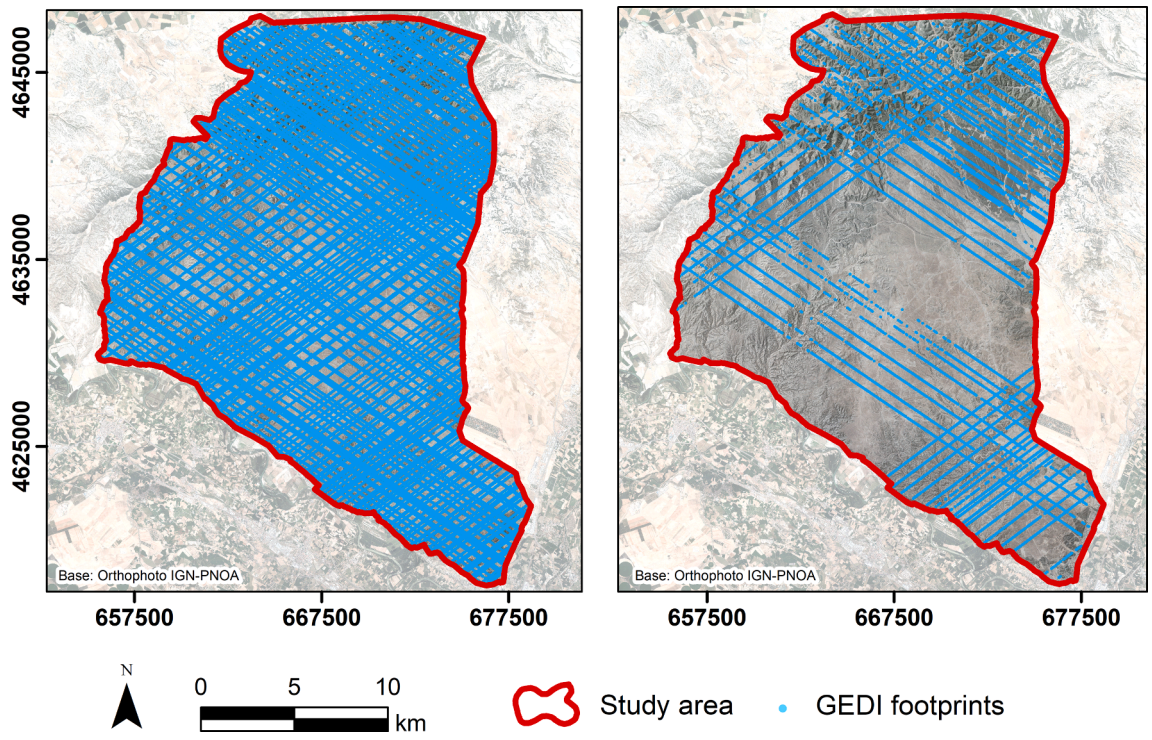

Fig. 3. Spatial location of the initial GEDI footprints (left) and the remaining GEDI footprints (right) after filtering.

each index, applying a circular buffer of 30 m radius to avoid GEDI geolocation uncertainty (Dubayah et al., 2021c).

2.4. Forest fuels ground-truth data

In order to assess GEDI for forest fuels modeling, the ground-truth data was obtained from two previous studies conducted in the same area to estimate and map *Prometheus* fuel types. The first was developed by Montealegre et al. (2015c) (thereafter, study 1), and the second was conducted by Revilla et al. (2021) (thereafter, study 2). Study 1 combined ALS-LiDAR data from PNOA and optical imagery from SPOT-5 satellite, acquired in 2011 and 2010, respectively, for spatializing the fuel types using Maximum Likelihood supervised classification method, obtaining an overall accuracy of 72.7 %. Study 2 assessed the suitability of the Discrete Anisotropic Radiative Transfer model DART (Gastellu-Etchegorry et al., 2016) to simulate low-density ALS-PNOA measurements and identify the fuel types. They selected the most highly correlated structural variables between the simulated and real ALS-PNOA data from 2016 using Spearman's rank correlation coefficient to classify the fuel types through Support Vector Machine, reaching overall accuracies of 91 % and 86 % using the simulated and real variables, respectively. To make this information more robust, as both data came from classification models with different global accuracies with uncertainties, it was decided to double-check both mappings, so that only footprints with the same fuel type in both studies were kept, being the ones that finally became part of the ground-truth. This caused an absence of fuel type FT6 and a very small sample size of FT5. It is important to highlight that the presence of these two fuel types was initially low, as some sectors of the study area were affected by forest fires in 1995 and 2008. In this sense, according to Domingo et al. (2020), these burned areas have a high density of shrubs that continue up to the tree strata (i.e., FT7). Furthermore, Gelabert et al. (2020) reported that differences in forest structure can be present in Aleppo pine stands after 21 years of a forest fire in Mediterranean environments.

Forest fuel estimations for study 1 were acquired in a raster file format, 10 m spatial resolution. For study 2, it was required to spatialize the model at 25 m grid resolution considering the size of the field plots of this study and GEDI footprint size. We extracted the mode of the pixel values (i.e., the fuel types) contained in each selected GEDI footprint using the same circular buffers as in previous steps. Furthermore, due to the smaller pixel size of study 1 compared to the GEDI footprint size, in order to ensure that the fuel type within each footprint was homogeneous, we only considered footprints with a fuel type mode exceeding a majority of 65 %. As a result, two *Prometheus* classes –one from study 1 and other from study 2– were assigned to each GEDI footprint. Finally, we did the selection of footprints with matching fuel types from both studies, resulting in a final sample of 1,112 footprints.

2.5. Classification of Prometheus fuel types and model validation

A primary selection of GEDI and Landsat-8 OLI variables for classification of *Prometheus* fuel types was performed using three approaches for non-parametric data. The Spearman's rank correlation coefficient, considered a good tool to determine relationship between LiDAR and ground-truth data (Kristensen et al., 2015), determined the direction and strength of the relationship between *Prometheus* fuel types and GEDI and Landsat-8 OLI data. The Kruskal-Wallis and the Dunn's tests determined if there were significant differences of each selected variable between the *Prometheus* fuel types. After comparing results from the three selection methods, the only one variable from L4A product was selected for input into the classification models along with one very significant variable from each of the products L2A and L2B, and the most significant variable from the multispectral indices. We only introduced one variable per GEDI product and multispectral indices in order to build parsimonious models and to avoid collinearity problems. Then, two classification methods were tested to classify *Prometheus* fuel types: Random Forest (RF), calculated using the R 'randomForest' (Liaw & Wiener, 2002) and 'caret' (Kuhn, 2008) packages, and Support Vector Machine (SVM), computed with both radial (SVM-R) and linear (SVM-L) kernels using the R package 'e1071′ (Meyer et al., 2020).After testing different combinations of parameters, RF models were parametrized with 500 trees and 2 metrics in each node, while SVM models were

tuned with a gamma value of 0.15 and a cost value of 500 and 100 for SVM-R and SVM-L, respectively. All explanatory variables were normalized before introducing them in the models.

Two classifications were performed: the first one including exclusively GEDI most suitable variables, and the second one integrating variables from first classification with the most relevant spectral index from Landsat-8 OLI. To validate the models, the dataset was split into training and test sets (80 % and 20 % of the cases, respectively), resulting in a relatively balanced distribution of each fuel type (Table 3). The overall accuracy and Cohen's Kappa (kappa) coefficients were used to assess and determine the best classification models in general terms, and the confusion matrices allowed us to assess the prediction accuracies of the different fuel types, considering the user's and producer's accuracies in classification, determined by the commission and omission errors, respectively (Pontius et al., 2008).

3. Results

3.1. Fuel type classification using GEDI variables

The variables selected by the Spearman correlation coefficients and the Kruskal-Wallis and the Dunn's tests to be introduced in the models were the relative height at the 85th percentile (RH85) and the PAI from the L2A and L2B products, respectively, along with the AGBD from the L4A product. Complete results of the variables selection are shown in the Supplementary Materials (Tables S1, S2, and S3). The best performances were obtained with RF and SVM-R, both reaching an overall accuracy of 61.54 %, with a kappa coefficient of 0.51. The lowest performance was obtained with SVM-L, with an overall accuracy of 57.46 % and a kappa coefficient of 0.45. Confusion matrices for the three classification methods showed an important confusion in shrub fuel types (FT2, FT3, and FT4) (Table 4). FT2 reached the lowest accuracy in shrub types, since many of them were misclassified in FT1. There was also a significant error in FT4, with most of cases being categorized in shrub types FT2 and FT3, but also in tree type FT7. Furthermore, the few samples of FT5 were inaccurately classified in FT7. On the contrary, there was better success on classification of FT1 and FT7. Complete results of the confusion matrices can be seen in Tables S4, S5, and S6 of the Supplementary Materials.

3.2. Fuel type classification using GEDI and Landsat-8 OLI variables

The brightness of Tasseled Cap transformation was the most suitable variable of the Landsat-8 OLI spectral indices for differentiating between *Prometheus* fuel types according to the Spearman correlation coefficients and the Kruskal-Wallis and the Dunn's tests (Tables S1, S2, and S3). It was therefore selected for input into the classification models along with the three most explanatory GEDI variables. The integration of the brightness with RH85, PAI, and the AGBD substantially improved the performance of the classification models, achieving an increase of 30 % of average accuracy using the combination of both data sources. Fig. 4 presents the distribution of the values of these four explanatory variables for the different *Prometheus* fuel types. It can be observed how the brightness is crucial to distinguish between fuel types FT1, FT2, and FT3, and between FT5 and FT7. The best performance was achieved with RF, reaching an overall accuracy of 83.71 %, with a kappa coefficient of 0.79. SVM models had slightly lower performances than RF, with an overall accuracy of 81.90 % and a kappa coefficient of 0.77 in the SVM-R model, and an overall accuracy of 81 % and a kappa coefficient of 0.76 in the SVM-L model.

Table 3
Number of training and test GEDI footprints and percentage (in brackets) of total GEDI footprints per *Prometheus* fuel type assigned for the classification models.

Dataset	FT1	FT2	FT3	FT4	FT5	FT7	Total
Training	211 (78 %)	177 (81 %)	173 (82 %)	150 (83 %)	11 (85 %)	169 (78 %)	**891 (80 %)**
Test	61 (22 %)	42 (19 %)	38 (18 %)	30 (17 %)	2 (15 %)	48 (22 %)	**221 (20 %)**
Total	272	219	211	180	13	217	**1,112**

Table 4
Comparison between Producer's accuracies and User's accuracies of *Prometheus* fuel types classification methods for the selected GEDI variables (RH85 + PAI + AGBD).

Fuel types	Producer's accuracy			User's accuracy		
	SVM-R	SVM-L	RF	SVM-R	SVM-L	RF
FT1	93.44 %	93.44 %	83.61 %	74.03 %	73.08 %	77.27 %
FT2	23.81 %	26.19 %	30.95 %	35.71 %	26.83 %	41.94 %
FT3	52.63 %	21.05 %	47.67 %	46.51 %	50.00 %	42.86 %
FT4	26.67 %	33.33 %	43.33 %	50.00 %	41.67 %	46.43 %
FT5	0.00 %	0.00 %	0.00 %	0.00 %	0.00 %	0.00 %
FT7	85.42 %	85.42 %	85.42 %	71.93 %	66.13 %	75.93 %

The integration of brightness produced less confusion in all fuel types, especially in the shrub fuels (FT2, FT3, and FT4) which had the highest confusion rates when only GEDI variables were introduced into the classification models. An improvement in omission error of 36.68 % was achieved, always exceeding the 50 % of hits in each fuel type (Table 5). FT2 was now the shrub type with the highest hit rates, whereas FT4 had the highest confusion. Few FT2 samples were incorrectly classified in FT1, while in FT3 confusion was found between FT2 and FT4, and some FT4 samples were misclassified in FT7. Nonetheless, integration of the brightness did not allow to correctly categorize the scarce samples of FT5, which were classified into FT7. The hit rates for the FT1 and FT7 fuel types improved by an average of 9 % and 2 %, respectively, with respect to the models using only GEDI variables, highlighting the very high hit rate in FT1, which reached a 100 % hit rate with both SVM classification methods. Finally, hit rates by fuel type were more balanced when classifying with RF than with SVM models. Complete results of the confusion matrices can be seen in Tables S7, S8, and S9 of the Supplementary Materials.

4. Discussion

This study reveals that GEDI provides useful information for classifying *Prometheus* fuel types using derived variables from the L2A, L2B, and L4A footprint data sets products. However, high rates of confusion were reported in shrub fuel types when only GEDI variables were included in the models, hinting certain limitations of the sensor that has been minimized by integrating multispectral data, in particular the brightness index from Landsat-8 OLI images, improving the overall accuracy of the models, as well as reducing the confusion between fuel types. Nevertheless, it should be considered the uncertainty of our ground-truth data, which was the result of classification models of *Prometheus* fuel types in two previous studies in the same area, influencing in the classification accuracy of our results.

A first and essential step was to filter the high uncertainty GEDI data to select the highest quality sample. We used the 'quality flag' attribute combined with other quality filters satisfactory used in previous GEDI-related studies, such as the removal of samples with degraded geolocation (e.g., Di Tommaso et al., 2021), acquired during the day time (e.g., Fayad et al., 2021a; Potapov et al., 2021), or with high land cover heterogeneity (e.g., Dorado-Roda et al., 2021). Many previous studies have also worked with only full-power laser beams (e.g., Potapov et al., 2021; Rishmawi et al., 2021), as coverage beams are underpowered and could produce inaccurate estimations. In this way, Duncanson et al. (2020) found higher RMSE values for coverage laser beams than full-power laser beams for biomass estimations using simulated GEDI data. However, we did not notice any improvement on our classification models by working only with full-power laser beams, so we used all laser beams in order to not reduce our sample size too much. In fact, the

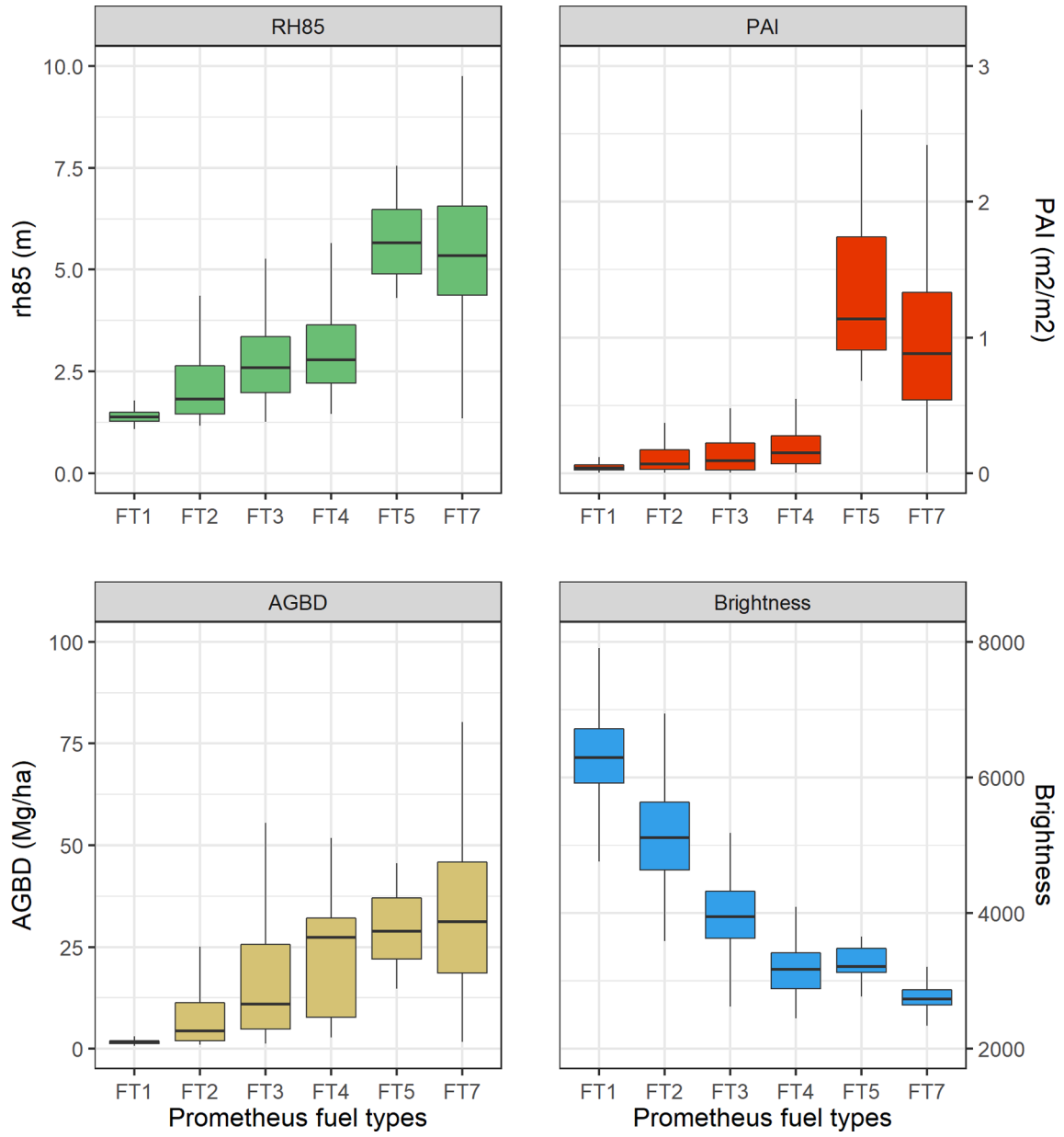

Fig. 4. Distribution values of the selected GEDI and Landsat-8 OLI variables for the *Prometheus* fuel types classification.

Table 5
Comparison between Producer's accuracies and User's accuracies of *Prometheus* fuel types classification methods for the selected GEDI and Landsat-8 OLI variables (RH85 + PAI + AGBD + Brightness).

Fuel types	Producer's accuracy			User's accuracy		
	SVM-R	SVM-L	RF	SVM-R	SVM-L	RF
FT1	100.00 %	100.00 %	96.72 %	89.71 %	88.41 %	92.19 %
FT2	78.57 %	69.05 %	85.71 %	89.79 %	87.88 %	81.82 %
FT3	71.05 %	73.68 %	71.05 %	72.97 %	70.00 %	79.41 %
FT4	60.00 %	63.33 %	63.33 %	62.07 %	63.33 %	70.37 %
FT5	0.00 %	0.00 %	0.00 %	0.00 %	0.00 %	0.00 %
FT7	87.50 %	87.50 %	91.67 %	85.71 %	85.71 %	86.27 %

filtering process led to work with 16 % of the initial footprints, similar to Lang et al. (2021) and Rishmawi et al. (2021), who retained ~ 28 % and ~ 11 % of the GEDI initial footprints in their filtering process, respectively.

The comparison between the three classification methods showed that RF and SVM-R had the highest performances for modeling *Prometheus* fuel types. RF has been used in several previous GEDI-related works (e.g., Di Tommaso et al., 2021; Fayad et al., 2021b; Leite et al., 2022; Liang et al., 2023; Rishmawi et al., 2021) but, to the best of our knowledge, none have used SVM yet, which has proven to be an efficient classification method in several previous studies using ALS-LiDAR data (e.g., Domingo et al., 2020; García et al., 2011; Jakubowksi et al., 2013). The overall accuracies of RF and SVM-R models using only GEDI variables were slightly better to the ones obtained by Domingo et al. (2020), who achieved overall accuracies of 57 % with SVM-R and 54 % with RF using only ALS-LiDAR variables. In this sense, the lower accuracy obtained by Domingo et al. (2020) could be due to the higher size of the study area that comprised a higher heterogeneity and complexity of the Mediterranean forests dominated by three species of pines, oaks, and Portuguese oaks. The inclusion of the brightness from Landsat-8 OLI imagery with the GEDI variables resulted in a substantial improvement in the classification models. Other authors had already noticed the good agreement between GEDI and multispectral imagery. For instance, Potapov et al. (2021) estimated global forest canopy height using both

GEDI and Landsat data. Rishmawi et al. (2021) extrapolated GEDI measurements at 1 km spatial resolution, by including the Visible Infrared Imaging Radiometer Suite instrument. Francini et al. (2022) analyzed multi-temporal Landsat imagery to monitor forest disturbances in Italy and observed that GEDI provided complementary information by being able to capture forest biomass changes due to that disturbances. Similarly, Liang et al. (2023) combined forest structural metrics from GEDI with Landsat spectral indices to quantify biomass losses over a 10-years period in Mozambique. Since this is the first study applied to classify forest fuels integrating GEDI with multispectral imagery, we cannot compare with similar previous studies, but our results confirm that it seems appropriate to integrate GEDI with multispectral sensors to obtain more robust results.

The classification of each fuel type showed the greatest confusion within the shrub fuel types (FT2, FT3, and FT4), being higher when the brightness was not integrated in the models. When exclusively using GEDI variables, RF had less confusion in shrub types with respect to SVM-R, which was quite high in FT2 in the latter. Confusion was also observed between FT4 and FT7, which is usual due to the vertical continuity of the strata in both types, making difficult to differentiate them, even in the field itself. In contrast, the error in FT1 and FT7, the best performing fuel types, was somewhat higher in RF than in SVM-R but both always showed high hit rates. Confusion between fuel types was substantially reduced when including the brightness, especially in the shrub fuel types, thus meaning that the combination of structure with spectral response of vegetation highlights forest attributes and allows better differentiation between *Prometheus* fuel types. When combining GEDI and Landsat, no omission errors were found in FT1 with both SVM models, and very few with RF. On the other hand, FT4 and FT7 were slightly better classified with RF. In addition, lower omission errors were found in FT2 when classifying with RF, although commission error were lower in SVM-R. The uncertainty associated with our ground-truth, which may have been propagated to our results leading to misclassifications of fuel types, must also be taken into account. In this way, study 1 found important confusions between FT2-FT3 and FT5-FT6, while in study 2 confusions were mainly located between FT5-FT6-FT7 and FT1-FT3. This could explain the confusion of the shrub strata and the complete misclassifications in FT5 in our case, since in both studies the confusion was significant. However, it is important to bear in mind that the number of initial samples of FT5 in our study was extremely low. In this sense, previous studies have also reported high confusion rates in shrub fuels using both discrete-return and full-waveform LiDAR sensors, and also in grassland fuel types, although this is not our case. For instance, Marino et al. (2016) noticed more error in fuel cover and height in mixed grassland and shrublands fuels using ALS data. Similarly, Domingo et al. (2020) obtained generally more confusion in the *Prometheus* shrub fuel types. Moreover, previous GEDI-related studies have found lower performances in herbaceous and shrublands fuels (e.g., Leite et al., 2022), as well as lower correlation coefficients in sparse forest types with predominance of shrub and herbaceous vegetation (e.g., Dorado-Roda et al., 2021). At this respect, Schneider et al. (2020) warned that worst model performances in lower strata may be due to the mixing of ground energy with energy returned from the understory. Leite et al. (2022) also suggest that spaceborne LiDAR signal may interact with lower strata less strongly than with tree strata. Regarding confusion in tree fuel types, the incorrect categorization of the few FT5 samples in FT7 are in accordance with other studies, such as Domingo et al. (2020) and Huesca et al. (2019). However, the absence of FT6 and the scarcity of FT5 samples does not allow us to conclude significant results between these fuel types. In this context, future studies should include significant sample sizes of FT5 and FT6 to test GEDI's performance in classifying *Prometheus* trees fuel types.

The present study has shown the usefulness of GEDI data and its combination with spectral indices to classify *Prometheus* fuel types in a Mediterranean forest environment dominated by Aleppo pine. Since GEDI is still a novel source of information, further research on the use of this system to estimate forest fuels is needed in order to increase the knowledge on its capabilities and limitations. Based on the successful results obtained by integrating GEDI with Landsat-8 OLI data, it may be of interest to explore the combination of GEDI variables with other remote sensing datasets, such as the NASA's ATLAS system, regional or national LiDAR surveys, SAR sensors or another multispectral data, which would be of great value to predict fire behavior in large areas in order to mitigate the negative effects of forest fires over environment.

5. Conclusions

This study has provided an initial evaluation of GEDI's ability to estimate *Prometheus* fuel types in Mediterranean forest environments using the GEDI footprint-level products L2A, L2B, and L4A of release version 2. In addition, we have assessed the effect of integrating Landsat-8 OLI spectral indices with GEDI variables for the improvement of classification models. A quality filtering process was applied to the GEDI data, and the Spearman's correlation coefficient and the Kruskal-Wallis and Dunn's tests were chosen to select the relevant variables for forest fuels modelling: RH85, PAI, and AGBD from GEDI, and the brightness from Landsat-8 OLI. RF and SVM with radial kernel were the best classification methods, showing a significantly better model performance integrating the brightness with the three GEDI variables. Overall, the classification of fuel types was less accurate for shrub fuels, with much confusion between these types of fuels when only GEDI variables were introduced in the models and being lower integrating multispectral information. Given the results obtained in this study, it has been proven that GEDI footprint-level variables are useful for forest fuels modeling in forested areas where there is no availability of other LiDAR data, or for estimating forest fuels at a large spatial extent.

Funding

This work was supported by the Spanish Ministry of Science, Innovation, and Universities through an FPU predoctoral contract granted to R.H. (FPU18/05027); by Centro Universitario de la Defensa, Academia General Militar, through the project GEDIFUEL (CUD2020-07); by the Government of Aragon (Geoforest S51_20R co-financed with FEDER "Construyendo Europa desde Aragón"); and by the European Union-NextGenerationEU through a Margarita Salas postdoctoral contract granted to D.D. (MS-240621).

CRediT authorship contribution statement

Raúl Hoffrén: Conceptualization, Methodology, Software, Validation, Formal analysis, Investigation, Data curation, Writing – original draft, Writing – review & editing. **María Teresa Lamelas:** Conceptualization, Methodology, Validation, Investigation, Resources, Data curation, Writing – original draft, Writing – review & editing. **Juan de la Riva:** Conceptualization, Methodology, Validation, Investigation, Resources, Writing – original draft, Writing – review & editing. **Darío Domingo:** Software, Investigation, Writing – review & editing. **Antonio Luis Montealegre:** Investigation, Resources, Writing – review & editing. **Alberto García-Martín:** Investigation, Writing – review & editing. **Sergio Revilla:** Resources, Writing – review & editing.

Declaration of Competing Interest

The authors declare that they have no known competing financial interests or personal relationships that could have appeared to influence the work reported in this paper.

Data availability

Data will be made available on request.

Appendix A. Supplementary data

Supplementary data to this article can be found online at https://doi.org/10.1016/j.jag.2022.103175.

References

Albini, F., 1976. Estimating wildfire behavior and effects. USDA Forest Service, Intermountain Forest and Range Experiment Station, General Technical Report INT-30, 92 pp.

Ashworth, A., Evans, D.L., Cookie, W.H., Londo, A., Collins, C., Neuenschwander, A., 2010. Predicting southeastern forest canopy heights and fire fuel models using GLAS data. Photogramm. Eng. Remote Sens. 76 (8), 915–922. https://doi.org/10.14358/PERS.76.8.915.

Decuyper, M., Chávez, R.O., Lohbeck, M., Lastra, J.A., Tsendbazar, N., Hackländer, J., Herold, M., Vågen, T.G., 2022. Continuous monitoring of forest change dynamics with satellite time series. Remote Sens. Environ. 269, 112829 https://doi.org/10.1016/J.RSE.2021.112829.

Di Tommaso, S., Wang, S., Lobell, D.B., 2021. Combining GEDI and Sentinel-2 for wall-to-wall mapping of tall and short crops. Environ. Res. Lett. 16 (12) https://doi.org/10.1088/1748-9326/ac358c.

Domingo, D., de la Riva, J., Lamelas, M.T., García-Martín, A., Ibarra, P., Echeverría, M., Hoffrén, R., 2020. Fuel type classification using airborne laser scanning and Sentinel-2 data in Mediterranean forest affected by wildfires. Remote Sens. 12 (21), 1–22. https://doi.org/10.3390/rs12213660.

Dorado-Roda, I., Pascual, A., Godinho, S., Silva, C.A., Botequim, B., Rodríguez-Gonzálvez, P., González-Ferreiro, E., Guerra-Hernández, J., 2021. Assessing the accuracy of GEDI data for canopy height and aboveground biomass estimates in Mediterranean forests. Remote Sens. 13 (12), 2279. https://doi.org/10.3390/rs13122279.

Dubayah, R., Blair, J.B., Goetz, S., Fatoyinbo, L., Hansen, M., Healey, S., Hofton, M., Hurtt, G., Kellner, J., Luthcke, S., Armston, J., Tang, H., Duncanson, L., Hancock, S., Jantz, P., Marselis, S., Patterson, P.L., Qi, W., Silva, C.A., 2020. The Global Ecosystem Dynamics Investigation: High-resolution laser ranging of the Earth's forests and topography. Science of Remote Sens. 1, 100002 https://doi.org/10.1016/j.srs.2020.100002.

Dubayah R., Hofton, M., Blair, J.B., Armston, J., Tang, H., Luthcke, S., 2020a. GEDI L2A Elevation and Height Metrics Data Global Footprint Level V001 . NASA EOSDIS Land Processes DAAC.

Dubayah, R., Hofton, M., Blair, J., Armston, J., Tang, H., Luthcke, S. 2021a. GEDI L2A Elevation and Height Metrics Data Global Footprint Level V002 . NASA EOSDIS Land Processes DAAC. Accessed 2022-12-08 from https://doi.org/10.5067/GEDI/GEDI02_A.002.

Dubayah, R., Tang, H., Armston, J., Luthcke, S., Hofton, M., Blair, J. 2021b. GEDI L2B Canopy Cover and Vertical Profile Metrics Data Global Footprint Level V002 [Data set]. NASA EOSDIS Land Processes DAAC. Accessed 2022-12-08 from https://doi.org/10.5067/GEDI/GEDI02_B.002.

Dubayah, R., Luthcke, S., Blair, J., Hofton, M., Armston, J., Tang, H. 2021c. GEDI L1B Geolocated Waveform Data Global Footprint Level V002 [Data set]. NASA EOSDIS Land Processes DAAC. Accessed 2022-12-08 from https://doi.org/10.5067/GEDI/GEDI01_B.002.

Dubayah, R., Armston, J., Kellner, J.R., Duncanson, L., Healey, S.P., Patterson, P.L., Hancock, S., Tang, H., Bruening, J., Hofton, M.A., Blair, J.B., Luthcke, S.B. 2022. GEDI L4A Footprint Level Aboveground Biomass Density, Version 2.1. ORNL DAAC, Oak Ridge, Tennessee, USA. https://doi.org/10.3334/ORNLDAAC/2056.

Duncanson, L., Neuenschwander, A., Hancock, S., Thomas, N., Fatoyinbo, T., Simard, M., Silva, C.A., Armston, J., Luthcke, S.B., Hofton, M., Kellner, J.R., Dubayah, R., 2020. Biomass estimation from simulated GEDI, ICESat-2 and NISAR across environmental gradients in Sonoma County. California. Remote Sens. Environ. 242 https://doi.org/10.1016/j.rse.2020.111779.

Evans, J.S., Hudak, A.T., 2007. A multiscale curvature algorithm for classifying discrete return LiDAR in forested environments. IEEE Trans. Geosci. Remote Sens. 45 (4), 1029–1038. https://doi.org/10.1109/TGRS.2006.890412.

Fayad, I., Baghdadi, N., Riedi, J., 2021a. Quality assessment of acquired GEDI waveforms: Case study over France. Tunisia and French Guiana. Remote Sens. 13, 3144. https://doi.org/10.3390/rs13163144.

Fayad, I., Ienco, D., Baghdadi, N., Gaetano, R., Alvares, C.A., Stape, J.L., Ferraço Scolforo, H., le Maire, G., 2021b. A CNN-based approach for the estimation of canopy heights and wood volume from GEDI waveforms. Remote Sens. Environ. 265 https://doi.org/10.1016/j.rse.2021.112652.

Ferraz, A., Saatchi, S., Mallet, C., Meyer, V., 2016. Lidar detection of individual tree size in tropical forests. Remote Sens. Environ. 183, 318–333. https://doi.org/10.1016/J.RSE.2016.05.028.

Flannigan, M.D., Stocks, B.J., Wotton, B.M., 2000. Climate change and forest fires. Sci. Total Environ. 262, 221–229. https://doi.org/10.1016/S0048-9697(00)00524-6.

Francini, S., D'Amico, G., Vangi, E., Borghi, C., Chirici, G., 2022. Integrating GEDI and Landsat: Spaceborne LiDAR and four decades of forest disturbances and biomass changes in Italy. Sensors 22, 2015. https://doi.org/10.3390/s22052015.

García, M., Riaño, D., Chuvieco, E., Salas, J., Danson, F.M., 2011. Multispectral and LiDAR data fusion for fuel type mapping using Support Vector Machine and decision rules. Remote Sens. Environ. 115 (6), 1369–1379. https://doi.org/10.1016/j.rse.2011.01.017.

García, M., Popescu, S., Riaño, D., Zhao, K., Neuenschwander, A., Agca, M., Chuvieco, E., 2012. Characterization of canopy fuels using ICESat/GLAS data. Remote Sens. Environ. 123, 81–89. https://doi.org/10.1016/j.rse.2012.03.018.

Gastellu-Etchegorry, J.P., Yin, T., Laurent, N., Grau, E., Rubio, J., Cook, B.D., Morton, D. C., Sun, G., 2016. Simulation of satellite, airborne and terrestrial LiDAR with DART (I): Waveform simulation with quasi-Monte Carlo ray tracing. Remote Sens. Environ. 184, 418–435. https://doi.org/10.1016/j.rse.2016.07.010.

Gelabert, P.J., Montealegre, A.L., Lamelas, M.T., Domingo, D., 2020. Forest structural diversity characterization in Mediterranean landscapes affected by fires using Airborne Laser Scanning data. GIScience Remote Sens. 57 (4), 497–509. https://doi.org/10.1080/15481603.2020.1738060.

Gorelick, N., Hancher, M., Dixon, M., Ilyushchenko, S., Thau, D., Moore, R., 2017. Google Earth Engine: Planetary-scale geospatial analysis for everyone. Remote Sens. Environ. 202, 18–27. https://doi.org/10.1016/J.RSE.2017.06.031.

Guerra-Hernández, J., Pascual, A., 2021. Using GEDI LiDAR data and Airborne Laser Scanning to assess height growth dynamics in fast-growing species: a showcase in Spain. For. Ecosyst. 8 (14) https://doi.org/10.1186/s40663-021-00291-2.

Hancock, S., Armston, J., Hofton, M., Sun, X., Tang, H., Duncanson, L.I., Kellner, J.R., Dubayah, R., 2019. The GEDI Simulator: A large-footprint waveform LiDAR simulator for calibration and validation of spaceborne missions. Earth Space Sci. 6, 294–310. https://doi.org/10.1029/2018EA000506.

Hofton, M., Blair, J.B., Story, S., Yi, D., 2019. Algorithm Theoretical Basis Document (ATBD) for GEDI transmit and receive waveform processing for L1 and L2 products. Goddard Space Flight Centre.

Huesca, M., Riaño, D., Ustin, S.L., 2019. Spectral mapping methods applied to LiDAR data: Application to fuel type mapping. Int. J. Appl. Earth Obs. Geoinf. 74, 159–168. https://doi.org/10.1016/j.jag.2018.08.020.

Huete, A.R., 1988. A Soil-Adjusted Vegetation Index (SAVI). Remote Sens. Environ. 25, 295–309. https://doi.org/10.1016/0034-4257(88)90106-X.

Jakubowksi, M.K., Guo, Q., Collins, B., Stepehns, S., Kelly, M., 2013. Predicting surface fuel models and fuel metrics using LiDAR and CIR imagery in a dense, mountainous forest. Photogramm. Eng. Remote Sens. 79 (1), 37–49. https://doi.org/10.14358/PERS.79.1.37.

Jiang, F., Zhao, F., Ma, K., Li, D., Sun, H., 2021. Mapping the forest canopy height in northern China by synergizing ICESat-2 with Sentinel-2 using a stacking algorithm. Remote Sens. 13 (8), 1535. https://doi.org/10.3390/rs13081535.

Kauth, R.J., Thomas, G.S., 1976. The Tasseled Cap—A Graphic Description of the Spectral-Temporal Development of Agricultural Crops as Seen by Landsat. Proceedings, Symposium on Machine Processing of Remotely Sensed Data, Purdue University, West Lafayette, IN, 29 June-1 July 1976, 41–51.

Kristensen, T., Naesset, E., Ohlson, M., Bolstad, P.V., Kolka, R., 2015. Mapping above- and below-ground carbon pools in boreal forests: The case for airborne LiDAR. PLOS ONE 10, e0138450.

Kuhn, M., 2008. Building Predictive Models in R Using the caret Package. Journal of Statistical Software 28 (5), 1–26. https://doi.org/10.18637/jss.v028.i05.

Lang, N., Kalischek, N., Armston, J., Schindler, K., Dubayah, R., Wegner, J.D., 2021. Global canopy height regression and uncertainty estimation from GEDI LiDAR waveforms with deep ensembles. Remote Sens. Environ. 268, 112760 https://doi.org/10.1016/j.rse.2021.112760.

Leite, R.V., Silva, C.A., Broadbent, E.N., do Amaral, C.H., Liesenberg, V., de Almeida, D. R.A., Mohan, M., Godinho, S., Cardil, A., Hamamura, C., de Faria, B.L., Brancalion, P.H.S., Hirsch, A., Marcatti, G.E., Dalla Corte, A.P., Zambrano, A.M.A., da Costa, M.B.T., Matricardi, E.A.T., da Silva, A.L., et al., 2022. Large scale multi-layer fuel load characterization in tropical savanna using GEDI spaceborne LiDAR data. Remote Sens. Environ. 268, 112764 https://doi.org/10.1016/j.rse.2021.112764.

Liang, M., Duncanson, L., Silva, J.A., Sedano, F., 2023. Quantifying aboveground biomass dynamics from charcoal degradation in Mozambique using GEDI Lidar and Landsat. Rem. Sens. Environ. 284, 113367 https://doi.org/10.1016/j.rse.2022.113367.

Liaw, A., Wiener, M., 2002. Classification and Regression by randomForest. R News 2 (3), 18–22.

Lin, X., Xu, M., Cao, C., Dang, Y., Bashir, B., Xie, B., Huang, Z., 2020. Estimates of forest canopy height using a combination of icesat-2/atlas data and stereo-photogrammetry. Remote Sens. 12 (21), 1–21. https://doi.org/10.3390/rs12213649.

Liu, H.Q., Huete, A.R., 1995. A feedback based modification of the NDVI to minimize canopy background and atmospheric noise. IEEE Trans. Geosci. Remote Sens. 33, 457–465. https://doi.org/10.1109/TGRS.1995.8746027.

Marino, E., Ranz, P., Tomé, J.L., Noriega, M.Á., Esteban, J., Madrigal, J., 2016. Generation of high-resolution fuel model maps from discrete airborne laser scanner and Landsat-8 OLI: A low-cost and highly updated methodology for large areas. Remote Sens. Environ. 187, 267–280. https://doi.org/10.1016/j.rse.2016.10.020.

Masek, J.G., Vermote, E.F., Saleous, N.E., Wolfe, R., Hall, F.G., Huemmrich, K.F., Gao, F., Kutler, J., Lim, T.-K., 2006. A Landsat surface reflectance dataset for North America, 1990–2000. IEEE Geosci. Remote Sens. Lett. 3 (1), 68–72. https://doi.org/10.1109/LGRS.2005.857030.

McGaughey, R.J., 2009. FUSION/LDV: Software for LIDAR Data Analysis and Visualization V.4.21. USDA Forest Service. Washington DC, USA.

Meyer, D., Dimitriadou, E., Hornik, K., Weingessel, A., Leisch, F., 2020. e1071: Misc Function of the Department of Statistics, Probability Theory Group (Formerly: E1071). TU Wien. R package version 1.7–11. Available at: https://CRAN.R-project.org/package=e1071 (accessed 20 Jun 2022).

Montealegre, A.L., Lamelas, M.T., de la Riva, J., 2015b. Interpolation routines assessment in ALS-derived Digital Elevation Models development for forestry applications. Rem. Sens. 7(7), 8631-8654, https://doi.org.10.3390/rs70708631.

Montealegre, A.L., Lamelas, M.T., García-Martín, A., de la Riva, J., Escribano, F., 2015c. Cartografía de modelos de combustible mediante combinación de imágenes LiDAR, SAR y ópticas en el Centro de Adiestramiento "San Gregorio". In Montealegre, A.L., Lamelas, M.T., de la Riva, J. Aplicaciones forestales de los datos LiDAR-PNOA en ambiente mediterráneo: su filtrado e interpolación y el modelado de parámetros estructurales con apoyo de trabajo de campo. PhD Thesis. https://zaguan.unizar.es/record/61353.

Montealegre, A.L., Lamelas, M.T., de la Riva, J., 2015a. A comparison of open-source LiDAR filtering algorithms in a Mediterranean forest environment. IEEE J. Sel. Top. Appl. Earth Obs. Remote Sens. 8 (8), 4072–4085. https://doi.org/10.1109/JSTARS.2015.2436974.

Montealegre, A.L., Lamelas, M.T., de la Riva, J., García-Martín, A., Escribano, F., 2016. Use of low points density ALS data to estimate stand-level structural variables in Mediterranean Aleppo pine forest. Forestry 89 (4), 373–382. https://doi.org/10.1093/forestry/cpw008.

Narine, L.L., Popescu, S.C., Malambo, L., 2019. Synergy of ICESat-2 and Landsat for mapping forest aboveground biomass with deep learning. Remote Sens. 11 (12), 1503. https://doi.org/10.3390/rs11121503.

Narine, L.L., Popescu, S.C., Malambo, L., 2020. Using ICESat-2 to estimate and map forest aboveground biomass: A first example. Remote Sens. 12 (11), 1824. https://doi.org/10.3390/rs12111824.

Oliveira, S., Oehler, F., San Miguel-Ayanz, J., Camia, A., Pereira, J.M.C., 2012. Modeling spatial patterns of fire occurrence in Mediterranean Europe using Multiple Regression and Random Forest. For. Ecol. Manag. 275, 117–129. https://doi.org/10.1016/j.foreco.2012.03.003.

Peterson, B., Nelson, K., Wylie, B., 2013. Towards Integration of GLAS into a National Fuel Mapping Program. Photogramm. Eng. Remote Sens. 2 (9), 175–183. https://doi.org/10.14358/PERS.79.2.175.

Pontius, R.G., Boersma, W., Castella, J.C., Clarke, K., de Nijs, T., Dietzel, C., Duan, Z., Fotsing, E., Goldstein, N., Kok, K., Koomen, E., Lippitt, C.D., McConnell, W., Sood, A. M., Pijanowski, B., Pithadia, S., Sweeney, S., Trung, T.N., Veldkamp, A.T., Verburg, P.H., 2008. Comparing the input, output, and validation maps for several models of land change. Ann. Reg. Sci. 42, 11–37. https://doi.org/10.1007/s00168-007-0138-2.

Potapov, P., Li, X., Hernández-Serna, A., Tyukavina, A., Hansen, M.C., Kommareddy, A., Pickens, A., Turubanova, S., Tang, H., Silva, C.A., Armston, J., Dubayah, R., Blair, J. B., Hofton, M., 2021. Mapping global forest canopy height through integration of GEDI and Landsat data. Remote Sens. Environ. 253, 112165 https://doi.org/10.1016/j.rse.2020.112165.

Prometheus,, 1999. Management techniques for optimization of suppression and minimization of wildfires effects. System Validation. European Commission, DG XII, ENVIR & CLIMATE, Contract Number ENV4-CT98-0716. European Commission, Luxembourg.

Puletti, N., Grotti, M., Ferrara, C., Chianucci, F., 2020. Lidar-based estimates of aboveground biomass through ground, aerial, and satellite observation: a case study in a Mediterranean forest. J. Appl. Remote Sens. 14 (4), 4501. https://doi.org/10.1117/1.jrs.14.044501.

R Core Team, 2020. R: A language and environment for statistical computing. R Foundation for Statistical Computing. Vienna, Austria. Available at: https://www.R-project.org/ (accessed 20 Jun 2022).

Renslow, M., 2013. Manual of Airborne Topographic Lidar. ASPRS, Bethesda, MD.

Revilla, S., Lamelas, M.T., Domingo, D., de la Riva, J., Montorio, R., Montealegre, A.L., García-Martín, A., 2021. Assessing the potential of the DART model to discrete return LiDAR simulation—Application to fuel type mapping. Remote Sens. 13 (3), 1–21. https://doi.org/10.3390/rs13030342.

Riaño, D., Chuvieco, E., Salas, J., Palacios-Orueta, A., Bastarrica, A., 2002. Generation of fuel type maps from Landsat TM images and ancillary data in Mediterranean ecosystems. Can. J. For. Res. 32, 1301–1315. https://doi.org/10.1139/x02-052.

Rishmawi, K., Huang, C., Zhan, X., 2021. Monitoring key forest structure attributes across the conterminous United States by integrating GEDI LiDAR measurements and VIIRS data. Remote Sens. 13 (3), 1–23. https://doi.org/10.3390/RS13030442.

Rothermel, C., 1972. A mathematical model for predicting fire spread in wildland fuels. Research Papers, INT-115. Ogden, UT: U.S. Department of Agriculture, Intermountain Forest and Range Experiment Station. 40 p.

Rouse, J.W., Haas, R.H., Schell, J.A., Deering, D.W., 1974. Monitoring Vegetation Systems in the Great Plains with ERTS. Third ERTS-1 Symposium NASA, NASA SP-351, Washington DC, 309–317.

Roy, D.P., Kashongwe, H.B., Armston, J., 2021. The impact of geolocation uncertainty on GEDI tropical forest canopy height estimation and change monitoring. Science of Remote Sens. 4, 100024 https://doi.org/10.1016/J.SRS.2021.100024.

Schneider, F.D., Ferraz, A., Hancock, S., Duncanson, L.I., Dubayah, R.O., Pavlick, R.P., Schimel, D.S., 2020. Towards mapping the diversity of canopy structure from space with GEDI. Environ. Res. Lett. 15 (11), 5006. https://doi.org/10.1088/1748-9326/ab9e99.

Silva, C.A., Duncanson, L., Hancock, S., Neuenschwander, A., Thomas, N., Hofton, M., Fatoyinbo, L., Simard, M., Marshak, C.Z., Armston, J., Lutchke, S., Dubayah, R., 2021. Fusing simulated GEDI, ICESat-2 and NISAR data for regional aboveground biomass mapping. Remote Sens. Environ. 253, 112234 https://doi.org/10.1016/j.rse.2020.112234.

Silva, C.A., Hamamura, C., Valbuena, R., Hancock, S., Cardil, A., Broadbent, E.N., Almeida, D.R.A., Silva Junior C.H.L., Klauberg, C., 2020. rGEDI: NASA's Global Ecosystem Dynamics Investigation (GEDI) data visualization and processing. version 0.1.8, Available at: https://github.com/carlos-alberto-silva/rGEDI (accessed 20 Jun 2022).